Nanoparticle Catalysts

International Edition: DOI: 10.1002/anie.201704632
German Edition: DOI: 10.1002/ange.201704632

Transition-Metal Nitride Core@Noble-Metal Shell Nanoparticles as Highly CO Tolerant Catalysts

*Aaron Garg, Maria Milina, Madelyn Ball, Daniela Zanchet, Sean T. Hunt, James A. Dumesic, and Yuriy Román-Leshkov**

Abstract: *Core–shell architectures offer an effective way to tune and enhance the properties of noble-metal catalysts. Herein, we demonstrate the synthesis of Pt shell on titanium tungsten nitride core nanoparticles (Pt/TiWN) by high temperature ammonia nitridation of a parent core–shell carbide material (Pt/TiWC). X-ray photoelectron spectroscopy revealed significant core-level shifts for Pt shells supported on TiWN cores, corresponding to increased stabilization of the Pt valence d-states. The modulation of the electronic structure of the Pt shell by the nitride core translated into enhanced CO tolerance during hydrogen electrooxidation in the presence of CO. The ability to control shell coverage and vary the heterometallic composition of the shell and nitride core opens up attractive opportunities to synthesize a broad range of new materials with tunable catalytic properties.*

Core–shell nanoparticles (NPs) represent a versatile design platform to simultaneously enhance the activity, increase the durability, and reduce the loading of noble metal (NM) catalysts. These materials exhibit significantly enhanced catalytic performance in a variety of reactions, including CO oxidation,[1] methanol oxidation (MOR),[2] and oxygen reduction (ORR)[3] when compared to their bulk counterparts. However, the broad applicability of such catalysts has been limited by the lack of independent control over the core and shell compositions, shell thickness, and particle size.[4] Furthermore, most core–shell catalysts are composed of shell materials that are fully miscible with the cores, resulting in metastable structures that restructure during heating or electrochemical cycling.[5]

Early-transition-metal carbides (TMCs) are ideal core materials owing to their earth-abundance, thermal stability, resistance to sintering, and chemical stability.[6] Notably, NMs form strong interfacial bonds with metal-terminated TMC surfaces yet are insoluble in the carbide lattice—a property that allows the NMs to coat the TMC surface while preventing alloying.[6,7] Transition-metal nitrides (TMNs) share all these favorable material properties of TMCs, but the additional valence electron in the N atom creates unique differences in the metal–ligand interaction. First, the increase in overall electron count affects the crystal structure as well as the number of d electrons available for bonding.[8] Second, the higher electronegativity of N compared to C results in greater charge transfer from the metal to N and less covalent mixing of valence orbitals.[8] While TMNs have been used for various reactions including hydrodenitrogenation,[9] hydrogenolysis,[10] alkane isomerization,[11] alkylation,[12] MOR,[13] and ORR,[14] they have rarely been investigated in core–shell materials owing to synthetic challenges that have precluded the effective deposition of thin NM shells on TMN NP cores (denoted as NM/TMN). To our knowledge, only a few examples of NM/TMN core–shell NPs, comprising Pt shells and TiN[15] or Group 8–10 (i.e., Fe, Co, Ni) TMN cores[16] have been reported.

Herein, we demonstrate the synthesis of early TMN NPs coated with thin NM layers, and we investigate the influence of the nitride core on the catalytic properties of the shell using coupled reactivity and characterization studies. Specifically, the effects of titanium tungsten nitride (denoted as TiWN) and titanium tungsten carbide (denoted as TiWC) cores on the electronic structure of Pt shells were compared using X-ray photoelectron spectroscopy (XPS). The hydrogen oxidation reaction (HOR) in the presence of CO was used to characterize the CO tolerance and to probe the observed differences in electronic structure. The results illustrate how the use of TMN cores offers an effective way to tune the reactivity of NM catalysts.

The synthesis of Pt/TiWN core–shell NPs is achieved by nitridation of Pt/TiWC NPs supported on carbon black (CB) under NH_3 flow at 800 °C (Figure 1). Recently, we developed a new high temperature self-assembly method to form NM/TMC NPs by carburizing silica encapsulated transition metal oxide NPs coated with NM salt precursors.[7] The porous silica template prevents the agglomeration of particles during the high temperature treatment and inhibits the nucleation of graphitic coke on the surface.[17] After dissolution of the silica in aqueous HF solution, the resulting core–shell NPs can be dispersed onto a high surface area support, such as CB. While a similar strategy can be followed to synthesize Pt/TiWN NPs by changing the 15 % CH_4/85 % H_2 carburizing atmosphere to an NH_3 nitriding atmosphere, the TiWN core is unstable during the silica removal process (Figure S1 in the Supporting

[*] A. Garg, M. Milina, Prof. D. Zanchet, S. T. Hunt, Prof. Y. Román-Leshkov
Department of Chemical Engineering
Massachusetts Institute of Technology
Cambridge, MA 02139 (USA)
E-mail: yroman@mit.edu
M. Ball, Prof. J. A. Dumesic
Department of Chemical and Biological Engineering
University of Wisconsin-Madison
Madison, WI 53706 (USA)
Prof. D. Zanchet
Institute of Chemistry, University of Campinas
Campinas, SP 13083-970 (Brazil)
Supporting information and the ORCID identification number(s) for the author(s) of this article can be found under: https://doi.org/10.1002/anie.201704632.

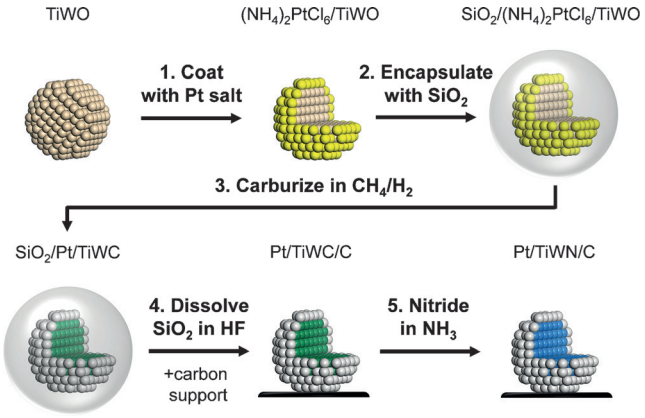

Figure 1. Schematic synthesis of Pt/TiWN core–shell NPs (beige TiWO, yellow $(NH_4)_2PtCl_6$, gray Pt, green TiWC, blue TiWN). Steps 1–4 depict the formation of Pt/TiWC core–shell NPs. Step 5 depicts the conversion of Pt/TiWC into Pt/TiWN.

Information). To circumvent this issue, we hypothesized that the sinter-resistance and strong interfacial bonds of Pt/TiWC NPs could be exploited to avoid particle agglomeration and to preserve the core–shell structure during the carbide-nitride conversion at 800 °C. While the transformation of TMNs into TMCs has been previously reported,[18] the conversion of a NM/TMC into a NM/TMN core–shell structure without disrupting the original architecture and particle size distribution (PSD) has not previously been demonstrated.

Evidence for the successful transformation of Pt/TiWC into Pt/TiWN NPs is shown in Figure 2. The parent carbide composition was $Ti_{0.2}W_{0.8}C$ as determined by inductively coupled plasma mass spectrometry (ICP-MS), and the nominal shell coverage was estimated to be on average 1 monolayer (ML) from a Pt to metal atomic ratio of 0.12 and a particle size of 5.2 nm.[19] The actual shell coverage, however, may vary among individual particles. The powder X-ray diffraction (PXRD) pattern for the parent Pt/TiWC NPs matched that of face-centered cubic (fcc) WC (PDF no. 00-020-1316) with a calculated lattice parameter of 0.422 nm (Figure 2a). The absence of reflections corresponding to fcc Pt indicated that Pt wets the TiWC surface and does not form separate particles. After nitridation at 800 °C for 3 h, the (111) reflection shifted from 37.0° to 37.7°, which is consistent with the contraction of the lattice from carbide to nitride. The PXRD pattern matched that of fcc W_2N (PDF no. 00-025-1257) with a calculated lattice parameter of 0.413 nm, suggesting complete nitridation. While the presence of a shoulder at 39.8° corresponding to Pt(111) indicates some restructuring of the Pt after nitridation, Rietveld refinement confirms that these fcc domains amount to only 18% of the total Pt and that the rest remains in a shell configuration undetectable by PXRD (Figure S2).

We also note that there was no statistically significant change in the particle size distribution as measured by transmission electron microscopy (TEM), demonstrating the exceptional resistance to sintering. Specifically, analysis of TEM images for 1 ML Pt/TiWN (Figure 2b) and 1 ML Pt/TiWC (Figure S3) yielded particle size distributions of 5.0 ± 1.3 nm and 5.2 ± 1.2 nm, respectively. In contrast, the PXRD pattern of commercial carbon-supported Pt NPs (denoted as

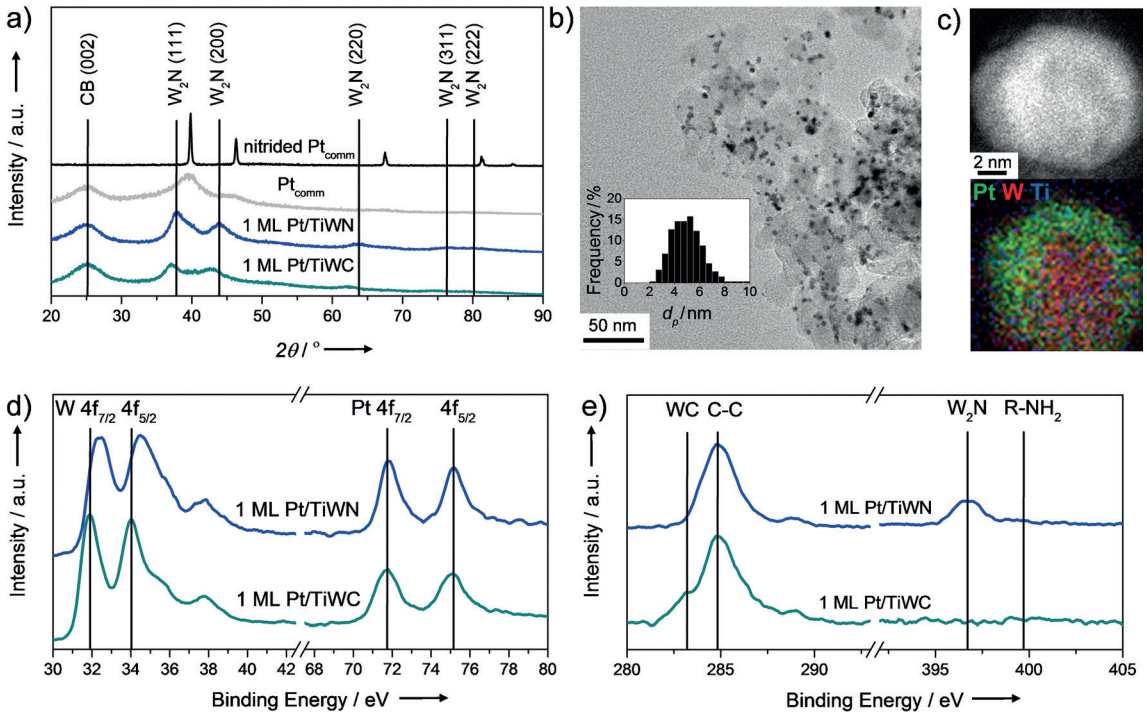

Figure 2. a) PXRD patterns of 1 ML Pt/TiWC and Pt_{comm} before and after nitridation. b) TEM image and particle size distribution of 1 ML Pt/TiWN. c) STEM-EDX map of a Pt/TiWN core–shell NP with a thicker shell. d) XPS spectra of 1 ML Pt/TiWC and after nitridation to 1 ML Pt/TiWN showing W 4f and Pt 4f signals. e) XPS spectra of unsupported 1 ML Pt/TiWC and after nitridation to 1 ML Pt/TiWN showing C 1s and N 1s signals.

Pt_{comm}, Premetek) after treatment under identical nitridation conditions showed sharp, narrow reflections indicating the presence of large, sintered Pt particles. For this material, the particle size distribution shifted from 2.1 ± 0.5 nm to 31.4 ± 20.5 nm after nitridation treatment, with some particles reaching over 100 nm (Figure S3). Scanning transmission electron microscopy paired with energy dispersive X-ray spectroscopy (STEM-EDX) was used to confirm the preservation of the core–shell structure for Pt/TiWN. Owing to low Pt signal, STEM-EDX mapping could only resolve clear Pt shells over a few ML thick (Figure 2c). However, STEM-EDX line scans indicated that the large majority of Pt exists in thin shells while 15% restructured to form Janus-like particles, which are the likely source of the Pt reflections in the PXRD pattern (Figure S4).

The elemental composition of the TiWN core was determined through a combination of ICP-MS and CHNS analysis. After accounting for the amount of N that can be incorporated into the CB support during nitridation, a stoichiometry of approximately $Ti_{0.2}W_{0.8}N_{0.6}$ was obtained. The stoichiometric coefficient of 0.6 for N for the heterometallic core is consistent with complete nitridation based on the 1:1 and 2:1 metal:N stoichiometry for the pure Ti and W nitride phases, respectively.[20] We suggest that the mechanism for the carbide to nitride transformation is analogous to that postulated by Volpe and Boudart for the carburization of W_2N and Mo_2N into WC_{1-x} and MoC_{1-x}.[18b] Given that Pt is unable to form a stable nitride (except at extremely high temperatures and pressures) as a result of its high degree of band-filling,[21] it remains completely insoluble in the TiWN lattice, which allows the core–shell structure to be maintained.

XPS was used to examine changes in chemical environment as well as surface composition (Figure 2d). After nitridation, the W $4f_{7/2}$ peak shifted from 31.9 to 32.4 eV, corresponding to a transition from carbide to nitride as N is more electronegative than C (W 4f peaks above 35 eV correspond to W^{6+} arising from surface passivation). Comparison of the surface atomic concentrations calculated by XPS to bulk atomic concentrations determined by ICP-MS revealed that Pt/TiWC and Pt/TiWN display similar levels of Pt enrichment at the surface, providing further evidence that the core–shell structure was preserved. For 1 ML Pt/TiWC, the ratio of surface Pt to metal, Pt/(Ti + W + Pt), was 0.20, and for 1 ML Pt/TiWN the ratio was 0.21, while the bulk Pt to metal ratio for both materials was 0.12. To confirm that C was removed from the lattice, unsupported 1 ML Pt/TiWC was subjected to identical nitridation conditions (Figure 2e). Without the CB support, it is possible to discern the presence of a carbidic C 1s peak at 283.1 eV in the XPS spectrum for 1 ML Pt/TiWC. After nitridation, the carbidic peak was undetectable and a nitridic N 1s peak at 396.8 eV was observed, indicating that all the interstitial C in the core was replaced by N. We note that adventitious carbon contamination was responsible for the peak observed at 284.8 eV in both samples.

The carbide to nitride conversion method was applied to core–shell NPs with varying Pt coverages (from 0.05 to 3 ML) using identical conditions to those used for the 1 ML case. The PXRD patterns after nitridation were consistent with fcc W_2N with a small contribution of fcc Pt, and STEM-EDX mapping confirmed that the core–shell structure was maintained for 2–3 ML Pt/TiWN (Figure S5). Analysis of TEM images before and after nitridation indicated similar PSDs for each coverage (Figure S6). Information about the Pt structure at varying coverages was obtained from extended X-ray absorption fine structure spectroscopy (EXAFS), which demonstrated changes in the coordination number consistent with the formation of thin shells (Figure S7 and Table S3).

XPS spectra for the core–shell nitrides and carbides at varying Pt coverages revealed clear trends for both the W 4f and Pt 4f binding energies (Figure 3). First, in all cases, the W 4f binding energies were shifted to higher values for the nitrides compared to carbides with equivalent Pt loading. Second, for both Pt/TiWN and Pt/TiWC, W 4f and Pt 4f peak binding energies decreased with Pt coverage. These shifts in core electron binding energy, called core level shifts (CLSs), have been observed for similar systems involving Pt and Pd overlayers on W substrates[22] and are indicative of the bonding interactions between Pt and W atoms resulting in a redistribution of charge that affects the core levels.[23]

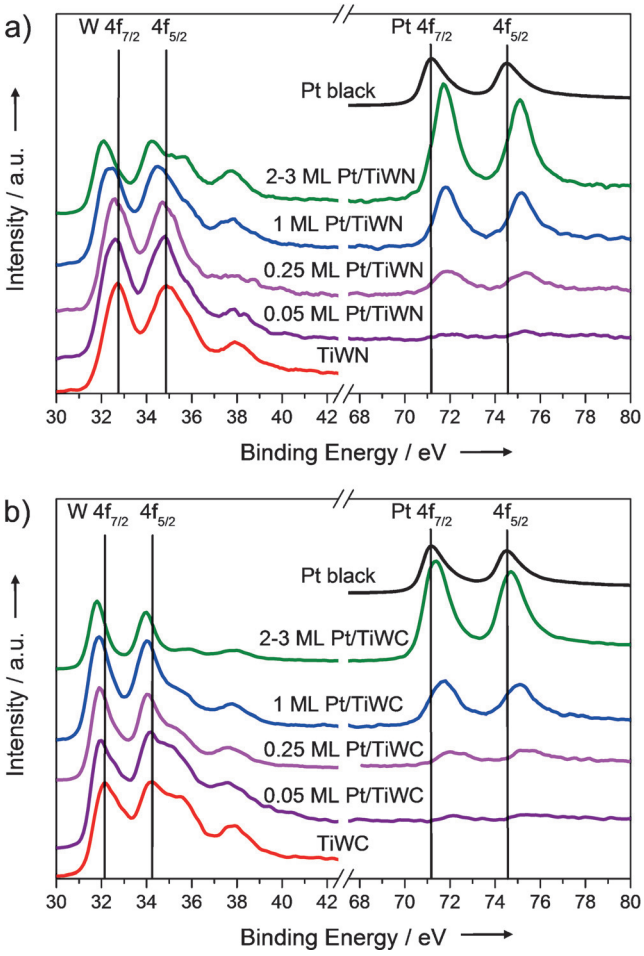

Figure 3. XPS spectra showing core level shifts for W 4f and Pt 4f binding energies of a) Pt/TiWN and b) Pt/TiWC at varying Pt coverages.

The magnitude and direction of the CLSs were calculated by comparing the Pt $4f_{7/2}$ and W $4f_{7/2}$ peaks in Pt/TiWN and Pt/TiWC to those of Pt black and either bare TiWN or TiWC (Table S4). For low Pt coverages, Pt/TiWN and Pt/TiWC displayed similar W $4f_{7/2}$ CLS and Pt $4f_{7/2}$ CLS values. At 0.05 ML, the Pt $4f_{7/2}$ CLS was approximately 0.9 eV and decreased to around 0.6 eV at 1 ML, in agreement with previous thin film studies involving Pt overlayers on W-based substrates.[22b,24] However, for the 2–3 ML Pt coverage, Pt/TiWN displayed W $4f_{7/2}$ and Pt $4f_{7/2}$ CLS values approximately 0.3 eV greater in magnitude than Pt/TiWC, suggesting that at higher coverages the nitride core may have a larger effect on the Pt electronic structure than the carbide. It should be noted that since the samples were conductive, charging was not observed to be an issue and thus no charge correction was needed or applied.

While it is clear that charge redistribution is responsible for the observed CLSs, the precise mechanism has been debated in the literature and may still be open to interpretation.[22a,23–25] The direction of the CLSs appear to indicate a charge transfer from the Pt shell to W in the core, which would result in a more attractive force on Pt electrons and more repulsive force on W electrons. However, examination of the work functions suggest a net transfer in the opposite direction, indicating that a simple interatomic charge transfer is inadequate in describing the CLSs for metal overlayer systems, as changes in the local potential around the core electrons arising from bonding and rehybridization can have a stronger effect on the binding energy than a net difference in charge on the overall atom.[23–25]

Although the exact cause is uncertain, these CLSs do demonstrate that the electronic and chemical properties of Pt are significantly altered by the presence of the TMC or TMN core and can also provide a measure of potential changes in the reactivity of Pt. Weinert and Watson showed that CLSs for metal overlayers are accompanied by similar shifts in the valence d-band center,[23] and Ontaneda et al. determined a near 1:1 correlation for core level and d-band shifts of Pd overlayers on Re.[25] Thus, the observed lower energy core electrons (higher XPS binding energy) of Pt in these core–shell materials should translate to a down-shifted d-band center compared to that of a pure Pt surface and consequently weaker adsorbate binding energies.[26] Indeed, CLSs of Group 10 metal overlayers on various substrates were found to correlate strongly with both the valence d-band center as well as the CO desorption temperature.[24] The larger CLSs for Pt/TiWN suggest that adsorbate binding will be even weaker for Pt/TiWN compared to Pt/TiWC.

To probe the difference in catalytic properties among our core–shell and commercial Pt catalysts, we characterized their CO tolerance by measuring the HOR activity in the presence of CO in 0.1 M $HClO_4$ using a rotating disk electrode (RDE) at 1600 rpm. The catalyst loadings on the electrode were targeted to have comparable Pt surface areas (Table S5), and all potentials are reported versus the reversible hydrogen electrode (RHE). HOR polarization curves for 2–3 ML Pt/TiWN, 2–3 ML Pt/TiWC, and Pt_{comm} showed that, in the absence of CO, all materials were excellent HOR catalysts, requiring overpotentials below 50 mV to reach the mass transfer limit (Figure 4a). In the presence of 1000 ppm of CO, the HOR activity of Pt_{comm} was suppressed until potentials above 0.5 V. In contrast, under identical conditions, both core–shell materials recovered their activity at potentials as low as 0.1 V, thus demonstrating remarkable CO tolerance, the cause of which is likely a combination of reduced CO binding energy and the adsorption of OH onto accessible W sites at low potentials. Notably, in agreement with the XPS CLSs data, Pt/TiWN displayed greater CO tolerance than Pt/TiWC as revealed by its higher initial activity over Pt_{comm} and Pt/TiWC, suggesting that CO binding is weakened such that oxidation of CO is facile even at 0.025 V and that the catalyst surface does not reach complete deactivation at these conditions.

CO stripping voltammograms (Figure 4b) showed large variations among the different catalysts, with the core–shell materials exhibiting a main peak near 0.8 V in addition to a pre-peak at a significantly lower potential near 0.3 V. While

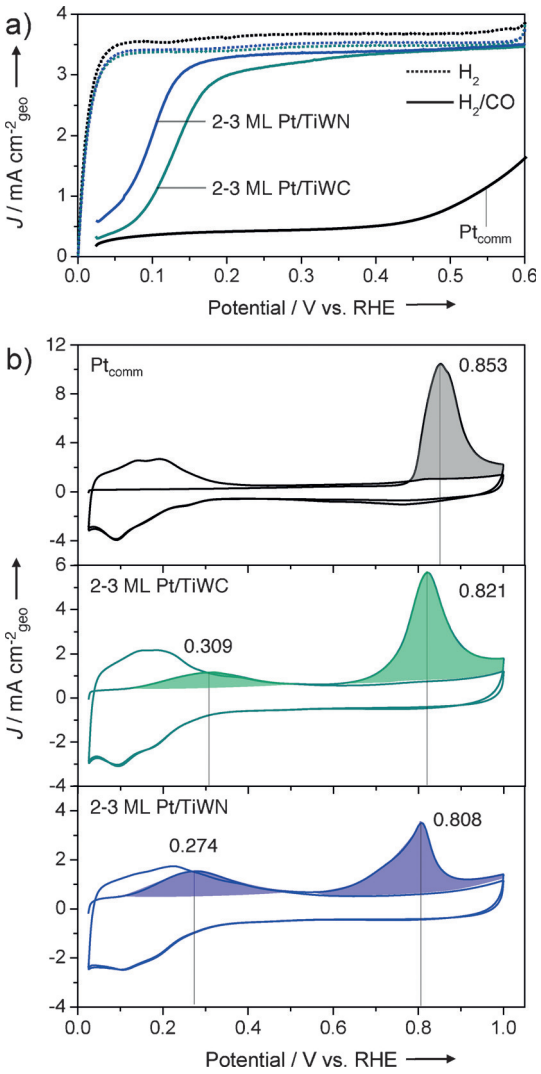

Figure 4. a) HOR polarization curves in H_2-saturated 0.1 M $HClO_4$ at 1600 rpm with and without 1000 ppm CO. b) CO stripping voltammograms in Ar-saturated 0.1 M $HClO_4$ at 1600 rpm after saturation with CO at 0.025 V versus RHE.

the role of adsorbed OH in initiating the reaction should not be discounted, previous work on Pt surfaces modified with W and Mo demonstrated that OH adsorption alone cannot be responsible for CO oxidation at low potentials.[27] Thus, the differences in CO stripping peak potentials may be attributed to differences in CO bond strength, with higher potentials corresponding to stronger binding.[28] For the core–shell materials, the two CO stripping regions likely correspond to different facets of the Pt shell, which can have varying d-band centers when supported on carbide or nitride cores.[29] Comparison of the pre-peak maxima for Pt/TiWN and Pt/TiWC at 0.274 and 0.309 V, respectively, indicates that Pt/TiWN binds CO even more weakly than Pt/TiWC. In addition, the difference in area of the pre-peaks suggests that Pt/TiWN has a higher percentage of weakly bound CO compared to Pt/TiWC (44% vs. 23%). These results provide direct evidence of the unique catalytic properties that arise by using a nitride core to modulate the electronic structure of Pt.

In summary, full conversion of Pt/TiWC NPs into Pt/TiWN NPs was achieved while preserving the core–shell structure. XPS spectra suggest greater stabilization of the Pt valence d-states for Pt/TiWN compared to Pt/TiWC, resulting in even higher CO tolerance from weakened binding strength. This effect indicates that Pt/TiWN core–shell materials would be desirable in catalytic applications where binding of adsorbates onto Pt is too strong and/or where poisoning is an issue. Lastly, the method to form Pt/TiWN core–shell NPs is general and can be applied to a range of NM/TMC systems with varying chemical composition, as evidenced by PXRD patterns and XPS spectra for PtPd/TiWN, Pt/TaTiWN, and Pt/NiWN that are consistent with core–shell structures (Figure S8). The versatility of this method demonstrates a promising way of synthesizing new core–shell architectures with tunable electronic properties to serve as next generation catalysts.

Experimental Section

Detailed procedures for the synthesis and characterization of materials are provided in the Supporting Information. Electrochemical measurements were performed at 30 °C on a RDE with a Ag/AgCl reference and platinum counter electrode. Catalyst inks were prepared by sonicating a mixture of deionized water, isopropanol, Nafion® 117 solution, and the carbon-supported catalyst. 6 μL of this ink was loaded onto freshly polished 3 mm glassy carbon disk electrodes and then dried to form the working electrode. HOR scans were performed in H_2-sat 0.1 M $HClO_4$ at 2 mV s^{-1} and 1600 rpm with iR compensation. To test CO tolerance, the working electrode was first held at 0.025 V until the electrolyte equilibrated with 1000 ppm CO before starting the HOR scan. To obtain the CO stripping voltammograms, the electrode was held at 0.025 V and 1600 rpm as the electrolyte was purged with CO to saturate the surface and then with Ar to remove excess CO. Immediately after, 3 CV scans were performed at 50 mV s^{-1}.

Acknowledgements

This work was supported by the U.S. Department of Energy, Office of Basic Energy Sciences (DE-SC0016214). S.T.H. thanks the National Science Foundation (Graduate Research Fellowship Grant No. 1122374), and M.M. thanks the Swiss National Science Foundation (Project No. P2EZP2_159124) for financial support. J.A.D and M.B. acknowledge use of facilities and instrumentation supported by the University of Wisconsin Materials Research Science and Engineering Center (DMR-1121288). J.A.D. acknowledges funding by the U.S. Department of Energy, Office of Basic Energy Sciences (DE-SC0014058). D.Z. acknowledges funding by the São Paulo Research Foundation (FAPESP 2015/23900-2 and 2015/50375-6) and the National Council of Technological and Scientific Development (CNPq 309373/2014-0). MRCAT operations are supported by the Department of Energy and the MRCAT member institutions. This research used resources of the Advanced Photon Source, a U.S. Department of Energy (DOE) Office of Science User Facility operated for the DOE Office of Science by Argonne National Laboratory under Contract No. DE-AC02-06CH11357 (10-BM-B beamline, GUP 52145) and the Brazilian Synchrotron Light Laboratory (XDS beamline, Proposal 20150214).

Conflict of interest

The authors declare no conflict of interest.

Keywords: carbides · CO tolerance · core–shell nanoparticles · electrocatalysis · nitrides

How to cite: *Angew. Chem. Int. Ed.* **2017**, *56*, 8828–8833
Angew. Chem. **2017**, *129*, 8954–8959

[1] S. Alayoglu, A. U. Nilekar, M. Mavrikakis, B. Eichhorn, *Nat. Mater.* **2008**, *7*, 333–338.
[2] D. Kaplan, M. Alon, L. Burstein, Y. Rosenberg, E. Peled, *J. Power Sources* **2011**, *196*, 1078–1083.
[3] K. Sasaki, H. Naohara, Y. Cai, Y. M. Choi, P. Liu, M. B. Vukmirovic, J. X. Wang, R. R. Adzic, *Angew. Chem. Int. Ed.* **2010**, *49*, 8602–8607; *Angew. Chem.* **2010**, *122*, 8784–8789.
[4] H. Yang, *Angew. Chem. Int. Ed.* **2011**, *50*, 2674–2676; *Angew. Chem.* **2011**, *123*, 2726–2728.
[5] a) C. S. Bonifacio, S. Carenco, C. H. Wu, S. D. House, H. Bluhm, J. C. Yang, *Chem. Mater.* **2015**, *27*, 6960–6968; b) C. Cui, L. Gan, M. Heggen, S. Rudi, P. Strasser, *Nat. Mater.* **2013**, *12*, 765–771; c) F. Tao, M. E. Grass, Y. Zhang, D. R. Butcher, J. R. Renzas, Z. Liu, J. Y. Chung, B. S. Mun, M. Salmeron, G. A. Somorjai, *Science* **2008**, *322*, 932–934.
[6] Y. Zhong, X. Xia, F. Shi, J. Zhan, J. Tu, H. J. Fan, *Adv. Sci.* **2016**, *3*, 1500286.
[7] S. T. Hunt, M. Milina, A. C. Alba-Rubio, C. H. Hendon, J. A. Dumesic, Y. Román-Leshkov, *Science* **2016**, *352*, 974–978.
[8] S. V. Didziulis, K. D. Butcher, *Coord. Chem. Rev.* **2013**, *257*, 93–109.
[9] J. C. Schlatter, S. T. Oyama, J. E. Metcalfe, J. M. Lambert, *Ind. Eng. Chem. Res.* **1988**, *27*, 1648–1653.
[10] V. Molinari, C. Giordano, M. Antonietti, D. Esposito, *J. Am. Chem. Soc.* **2014**, *136*, 1758–1761.
[11] M. K. Neylon, S. Choi, H. Kwon, K. E. Curry, L. T. Thompson, *Appl. Catal. A* **1999**, *183*, 253–263.
[12] W. Yao, P. Makowski, C. Giordano, F. Goettmann, *Chem. Eur. J.* **2009**, *15*, 11999–12004.
[13] M. Yang, Z. Cui, F. J. DiSalvo, *Phys. Chem. Chem. Phys.* **2013**, *15*, 1088–1092.

[14] a) J. Luo, X. Tian, J. Zeng, Y. Li, H. Song, S. Liao, *ACS Catal.* **2016**, *6*, 6165 – 6174; b) R. Ohnishi, K. Takanabe, M. Katayama, J. Kubota, K. Domen, *J. Phys. Chem. C* **2013**, *117*, 496 – 502.
[15] X. Tian, J. Luo, H. Nan, H. Zou, R. Chen, T. Shu, X. Li, Y. Li, H. Song, S. Liao, R. R. Adzic, *J. Am. Chem. Soc.* **2016**, *138*, 1575 – 1583.
[16] a) J. Hu, K. Kuttiyiel, K. Sasaki, D. Su, T. H. Yang, G. G. Park, C. Zhang, G. Chen, R. Adzic, *Catalysts* **2015**, *5*, 1321 – 1332; b) K. A. Kuttiyiel, K. Sasaki, Y. Choi, D. Su, P. Liu, R. R. Adzic, *Nano Lett.* **2012**, *12*, 6266 – 6271.
[17] S. T. Hunt, T. Nimmanwudipong, Y. Román-Leshkov, *Angew. Chem. Int. Ed.* **2014**, *53*, 5131 – 5136; *Angew. Chem.* **2014**, *126*, 5231 – 5236.
[18] a) J. B. Claridge, A. P. E. York, A. J. Brungs, M. L. H. Green, *Chem. Mater.* **2000**, *12*, 132 – 142; b) L. Volpe, M. Boudart, *J. Solid State Chem.* **1985**, *59*, 348 – 356.
[19] S. T. Hunt, M. Milina, Z. Wang, Y. Román-Leshkov, *Energy Environ. Sci.* **2016**, *9*, 3290 – 3301.
[20] a) S. Asgary, M. R. Hantehzadeh, M. Ghoranneviss, A. Boochani, *Rare Met.* **2016**, 1 – 9; b) S. Yu, Q. Zeng, A. R. Oganov, G. Frapper, L. Zhang, *Phys. Chem. Chem. Phys.* **2015**, *17*, 11763 – 11769.
[21] S. T. Oyama, *The Chemistry of Transition Metal Carbides and Nitrides*, Blackie, Glasgow, **1996**, p. 3.
[22] a) R. A. Campbell, J. Rodriguez, D. W. Goodman, *Surf. Sci.* **1990**, *240*, 71 – 80; b) D. V. Esposito, S. T. Hunt, Y. C. Kimmel, J. G. Chen, *J. Am. Chem. Soc.* **2012**, *134*, 3025 – 3033.
[23] M. Weinert, R. E. Watson, *Phys. Rev. B* **1995**, *51*, 17168 – 17180.
[24] J. Rodriguez, *Surf. Sci.* **1996**, *345*, 347 – 362.
[25] J. Ontaneda, R. A. Bennett, R. Grau-Crespo, *J. Phys. Chem. C* **2015**, *119*, 23436 – 23444.
[26] J. R. Kitchin, J. K. Nørskov, M. A. Barteau, J. G. Chen, *J. Chem. Phys.* **2004**, *120*, 10240 – 10246.
[27] a) G. Samjeské, H. Wang, T. Löffler, H. Baltruschat, *Electrochim. Acta* **2002**, *47*, 3681 – 3692; b) T. Nagel, N. Bogolowski, G. Samjeske, H. Baltruschat, *J. Solid State Electrochem.* **2003**, *7*, 614 – 618.
[28] A. C. Garcia, V. A. Paganin, E. A. Ticianelli, *Electrochim. Acta* **2008**, *53*, 4309 – 4315.
[29] C. H. Hendon, S. T. Hunt, M. Milina, K. T. Butler, A. Walsh, Y. Román-Leshkov, *J. Phys. Chem. Lett.* **2016**, *7*, 4475 – 4482.

Manuscript received: May 4, 2017
Accepted manuscript online: May 25, 2017
Version of record online: June 23, 2017

